Systematics of the low-energy pionic double charge exchange in nuclei

J. Draeger, R. Bilger,* H. Clement, M. Cröni, H. Denz, J. Gräter,† R. Meier, J. Pätzold, D. Schapler,‡
G. J. Wagner, and O. Wilhelm§
Physikalisches Institut der Universität Tübingen, Morgenstelle 14, D-72076 Tübingen, Germany

K. Föhl
Department of Physics and Astronomy, University of Edinburgh, Edinburgh, United Kingdom

M. Schepkin
Institute of Theoretical and Experimental Physics, Moscow, Russia
(Received 24 July 2000; published 20 November 2000)

The experimental results for the (π^+,π^-) reaction on nuclei obtained in recent years reveal clear systematic features of this reaction. New data on ^{7}Li, ^{12}C, ^{16}O, and ^{56}Fe supplementing the existing data base are presented. The data on ^{12}C are partly at variance with previous results. The dependence of the cross sections on incident energy, scattering angle, and on the target mass is discussed for transitions leading to the ground state of the final nucleus or to the double isobaric analog state.

PACS number(s): 25.80.Gn, 24.30.Gd, 14.20.Pt

I. INTRODUCTION

By charge conservation the pionic double charge exchange (DCX) on nuclei has to involve at least two nucleons in a nucleus. Hence, already to lowest order this reaction is a two-nucleon process. Consequently a high sensitivity of this reaction to nucleon-nucleon correlations is expected. That this is indeed the case, in particular at incident pion energies below the Δ resonance, has been shown in a number of theoretical investigations, for a survey see recent DCX reviews [1]. Of course, as a consequence of the second-order character of this reaction the cross sections are very low in the range of $nb-\mu b$, thus putting high demands on their measurements. On the other hand, this feature in combination with the high sensitivity to short-range correlations has since long been considered especially attractive to search for exotic phenomena like six-quark correlations [2] in nuclei. The interest further increased when contrary to previous theoretical predictions the experimentally observed forward angle cross sections were found to consistently exhibit a resonancelike energy dependence with a maximum about 40 MeV above threshold. This is close to the energy, where the forward angle single charge exchange reaction exhibits a deep minimum due to the well-known destructive isovector sp-wave interference in the πN system. Consequently, initial DCX calculations [3,4] predicted a dip rather than a bump at these energies, until one realized that inclusion of distortions, double spinflip, and/or coupled-channel effects could wash out this dip and even produce some kind of bump in such calculations [3–7]. In general, however, the agreement with data was modest.

The intriguing energy dependence in the data together with the established high sensitivity to short-range phenomena lead to the hypothesis of the formation of a narrow dibaryon resonance in the πNN channel, the so-called d' with $I(J^P)=$ even (0^-) and $m_{d'}\approx 2.06$ GeV [8,9]. Such a resonance must be NN decoupled, as otherwise a huge width due to the fall-apart decay into the NN channel would be observed. Indeed, with the adjustment of its total vacuum width $\Gamma_{\pi NN}\approx 0.5$ MeV and its spreading width $\Gamma_s\approx 10-20$ MeV due to collision damping all known data for transitions to the double isobaric analog state (DIAT) or the nonanalog ground state (GST) in the final nucleus could be described reasonably well [8–12] both in their angular and energy dependence. Only very recently a theoretical work [13] based on a conventional reaction mechanism succeeded for the first time in describing adequately both the observed energy and the angular dependences for the case of the Ca isotopes by fine tuning the optical model parameters and assuming the intermediate π^0 to propagate on mass shell in an optical potential.

The possible involvement of exotic processes in the low energy DCX has stimulated a number of new measurements [10–12,14] on nuclei across the periodic table, so that now a number of systematic features of the low-energy DCX emerge, which were not available previously. These will be discussed in the following together with new results on ^{7}Li, ^{12}C, ^{16}O, and ^{56}Fe supplementing the hitherto existing data base on these nuclei.

II. EXPERIMENTAL RESULTS

The new data on ^{7}Li, ^{12}C, ^{16}O, and ^{56}Fe have been taken at PSI with the LEPS setup [15] in very much the same way as has been the case for the previous measurements on ^{7}Li [12], ^{16}O [10], ^{34}S [16] ^{40}Ca [10], ^{56}Fe [8,16], ^{93}Nb [11], and ^{128,130}Te [14]. These data for pion energies $T_\pi \lesssim 90$ MeV are given in Table I. They complement earlier low-energy data taken at TRIUMF for ^{14}C [17], ^{18}O, and

*Present address: Landesbank BW, Stuttgart, Germany.
†Present address: Andersen Consulting, Munich, Germany.
‡Present address: SAP, Walldorf, Germany.
§Present address: Institut für Hochbautechnik, ETH Zürich, Switzerland.

TABLE I. DCX cross sections measured with the LEPS spectrometer at PSI for nonanalog ground state transitions (GST), transitions to the double isobaric analog state (DIAT), and nonanalog transitions to 0_2^+ and 0_3^+ states in the final nucleus.

Target nucleus	T_π [MeV]	Θ_{lab}	$\sigma(\Theta)$ [nb/sr] GST	0_2^+	0_3^+	DIAT	Remarks
^{7}Li	29.3	30.4°	72(31)				Ref. [12]
		45.2°	51(34)				– ‘‘ –
	39.4	17.6°	171(85)				– ’’ –
		30.4°	190(41)				– ‘‘ –
		45.2°	93(39)				– ’’ –
	43.8	30.4°	202(37)				– ‘‘ –
	51.2	17.6°	203(51)				– ’’ –
		30.4°	110(26)				– ‘‘ –
		45.2°	176(43)				– ’’ –
	54.6	17.6°	198(59)				– ‘‘ –
		30.4°	158(32)				– ’’ –
		45.2°	98(34)				– ‘‘ –
		65.1°	85(23)				– ’’ –
	59.5	17.6°	97(42)				– ‘‘ –
		30.4°	153(26)				– ’’ –
		45.2°	67(28)				– ‘‘ –
	63.9	30.4°	133(37)				– ’’ –
		45.2°	90(23)				– ‘‘ –
	69.0	17.6°	97(37)				– ’’ –
		30.4°	123(30)				– ‘‘ –
			97(37)				this work
		45.2°	120(37)				Ref. [12]
		65.1°	61(20)				this work
		90.0°	57(9)				– ’’ –
	78.8	30.4°	70(30)				Ref. [12]
		45.2°	180(66)				– ‘‘ –
	90.6	30.4°	70(35)				– ’’ –
		45.2°	114(64)				– ‘‘ –
^{12}C	49.8	30.4°	279(36)				this work
	53.9	30.4°	415(37)				– ’’ –
		45.2°	376(36)				– ‘‘ –
	59.5	30.4°	434(44)				– ’’ –
		45.2°	343(27)				– ‘‘ –
	64.6	30.4°	606(58)				– ’’ –
		45.2°	522(51)				– ‘‘ –
	69.7	17.6°	700(100)				– ’’ –
		30.4°	883(86)				– ‘‘ –

TABLE I. *(Continued).*

Target nucleus	T_π [MeV]	Θ_{lab}	$\sigma(\Theta)$ [nb/sr] GST	0_2^+	0_3^+	DIAT	Remarks
		45.2°	493(42)				– ’’ –
		65.1°	391(36)				– ‘‘ –
	79.6	30.4°	762(60)				– ’’ –
			626(60)				– ‘‘ –
		45.2°	446(48)				– ’’ –
		65.1°	305(49)				– ‘‘ –
	89.8	30.4°	374(46)				– ’’ –
			498(76)				– ‘‘ –
		45.2°	346(42)				– ’’ –
		65.1°	192(38)				– ‘‘ –
^{16}O	50.1	30.4°	192(32)	38(32)			Ref. [10]
		45.2°	79(33)	62(47)			– ’’ –
	54.5	30.4°	222(38)	34(33)			– ‘‘ –
		45.2°	144(22)	78(21)			– ’’ –
	59.9	30.4°	343(21)	125(15)			– ‘‘ –
		45.2°	205(23)	121(24)			– ’’ –
	64.8	17.6°	564(92)	217(62)			– ‘‘ –
		30.4°	453(32)	209(21)			– ’’ –
			476(21)	197(16)			this work
		45.2°	241(37)	112(19)			Ref. [10]
		651°	159(19)	80(15)			– ‘‘ –
	69.9	30.4°	431(30)	121(18)			– ’’ –
		45.2°	260(47)	113(36)			– ‘‘ –
	74.6	30.4°	368(18)	116(23)			– ’’ –
		45.2°	285(34)	46(21)			– ‘‘ –
	79.6	30.4°	243(18)	86(12)			– ’’ –
		45.2°	258(34)	43(32)			– ‘‘ –
	89.5	30.4°	199(30)	22(22)			– ’’ –
			139(40)	44(34)			this work
		45.2°	132(21)	23(21)			Ref. [10]
^{40}Ca	44.1	30.4°	260(54)				– ‘‘ –
	49.5	17.6°	605(156)				– ’’ –
		30.4°	334(43)				– ‘‘ –
		45.2°	268(50)				– ’’ –
		65.1°	130(25)				– ‘‘ –
	56.4	17.6°	575(93)				– ’’ –
		30.4°	417(50)				– ‘‘ –
		45.2°	332(40)				– ’’ –
		65.1°	101(19)				– ‘‘ –

TABLE I. *(Continued).*

Target nucleus	T_π [MeV]	Θ_{lab}	$\sigma(\Theta)$ [nb/sr] GST	0_2^+	0_3^+	DIAT	Remarks
	63.1	30.4°	479(60)				– ’’ –
		45.2°	161(22)				– ‘‘ –
	74.3	30.4°	222(41)				– ’’ –
	83.2	30.4°	64(31)				– ‘‘ –
^{56}Fe	33.5	30.4°	230(110)			230(160)	Ref. [8]
		45.2°	180(130)			190(190)	– ’’ –
	35.8	17.6°	268(200)	266(141)	324(123)	1056(328)	this work
		30.4°	215(60)	65(38)	64(38)	514(162)	– ‘‘ –
		45.2°	147(44)	34(26)	55(33)	460(151)	– ’’ –
	41.7	17.6°	331(106)	278(89)	177(85)	1024(262)	– ‘‘ –
		30.4°	301(36)	112(32)	142(34)	638(79)	– ’’ –
		45.2°	165(43)	124(49)	112(37)	528(119)	– ‘‘ –
	45.0	30.4°	243(42)	110(22)	147(37)	639(93)	– ’’ –
		45.2°	147(23)	49(16)	76(19)	355(44)	– ‘‘ –
	48.7	17.6°	427(78)	164(49)	253(53)	405(87)	– ’’ –
		30.4°	237(28)	117(20)	149(21)	354(30)	– ‘‘ –
			258(45)	175(34)	156(33)	654(82)	Ref. [16] [a]
		45.2°	77(24)	55(20)	76(23)	486(70)	– ’’ –
		65.1°	20(12)	19(11)	19(11)	221(48)	– ‘‘ –
	51.9	30.4°	155(30)	124(31)	125(28)	331(55)	this work
		45.2°	58(13)	48(15)	50(13)	234(37)	– ’’ –
	55.4	30.4°	146(23)	117(25)	76(19)	242(40)	– ‘‘ –
		45.2°	24(11)	11(8)	15(8)	102(26)	– ’’ –
	59.5	30.4°	81(33)			178(49)	Ref. [8]
		45.2°	27(9)			63(20)	– ‘‘ –
	83.0	30.4°	22(11)			47(36)	this work
^{93}Nb	30	30.4°	54(38)				Ref. [11]
	39.6	17.6°	255(82)				– ’’ –
		30.4°	118(27)				– ‘‘ –
	44.2	17.6°	237(86)				– ’’ –
		30.4°	122(25)				– ‘‘ –
		45.2°	34(19)				– ’’ –
		65.1°	21(21)				– ‘‘ –
	49.1	17.6°	128(59)				– ’’ –
		30.4°	59(14)			520(90)	– ‘‘ –
	60.0	30.4°	9(5)				– ’’ –

[a]Corrected values (see text).

^{56}Fe [18] and at LAMPF for ^{12}C [19], ^{14}C [20], ^{40,42,44,48}Ca [21–25], ^{56}Fe [25], and ^{93}Nb [25]. For target nuclei with isospin $I \geqslant 2$ data are available both for transitions to the ground state (GST) and to the double isobaric analog state (DIAT) in the final nucleus. For $I=1$ the GST is identical to the DIAT, whereas for $I=0$ nuclei there are no DIATs and the GSTs are of nonanalog character.

There are only a few data points which have been taken both at LAMPF and PSI on the same target nucleus at comparable energies and angles: The LAMPF data on ^{56}Fe [25] at $T_\pi=50$ MeV and $\Theta=25°$ agree well within statistics with the LEPS data both for GST and DIAT. This also holds for the GST on ^{40}Ca although the LAMPF data there [24] are of very poor statistical significance. In contrast, the cross section on ^{93}Nb [25] for the DIAT at $T_\pi=50$ MeV and $\Theta=35°$ is larger by a factor of 4, and the one on the ^{12}C [19] GST at $T_\pi=80$ MeV and $\Theta=35°$ measured at LAMPF is smaller by a factor of about 4 than the LEPS results, whereas the ^{12}C data at $T_\pi=60$ MeV are again in agreement with each other at all angles (see Fig. 3). The reasons for these huge discrepancies are unknown.

Figure 1 shows the experimental forward angle ($\Theta=5°$) cross sections for the nonanalog GSTs on ^{7}Li, ^{12}C, ^{16}O, ^{40}Ca, ^{56}Fe, and ^{93}Nb for $T_\pi \lesssim 300$ MeV. The data for $T_\pi \geqslant 100$ MeV are from LAMPF [26–31], whereas the data at lower energies are from PSI taken with LEPS. In order to allow comparison to the LAMPF data, the LEPS data have been extrapolated to $\Theta=5°$ by use of the data obtained in the range $17° \leqslant \Theta \leqslant 90°$. For ^{7}Li, ^{12}C, and ^{56}Fe the measured angular distributions are shown in Figs. 2–4. The error bars shown in Fig. 1 include uncertainties resulting from various extrapolation methods for monopole transitions assuming $\sigma(\Theta) \sim j_0(b\Theta)$ or $\sigma(\Theta) \sim \exp[b(\cos\Theta - 1)] - c$ [16,20–22] or $\sigma(\Theta)$ according to d' model predictions (see Sec. III). Generally, the latter method has been used for convenience (see curves shown in Figs. 2–4 and in Refs. [10,11]), however we would like to point out that all three extrapolation methods lead to the same value at $\Theta=5°$ within quoted uncertainties, as soon as more than two angles have been measured per energy. For the values put in brackets in Fig. 1 (for ^{40}Ca and ^{56}Fe at $T_\pi=83$ MeV), where only a single cross section per energy has been measured, see the discussion in the next section.

The new data for ^{7}Li (Fig. 2, star symbols) fit very well to our previous values [12] and extend the measured angular distribution at $T_\pi=70$ MeV up to 90°. They exhibit a surprisingly flat angular dependence at this energy, much flatter than expected from a diffraction behavior (dashed curves in Fig. 2), which is in accordance with the data below $T_\pi=70$ MeV, i.e., at energies across the low energy structure in the forward angle cross section (Fig. 1). A similar situation is indicative in the data for ^{12}C (Fig. 3), where the measured angular distribution at $T_\pi=90$ MeV appears to be somewhat flatter than expected from the diffraction model calculations (dashed curves in Fig. 3). The same situation is noted also in the ^{16}O data at $T_\pi=80,90$ MeV (see Table I).

For ^{56}Fe the new data are plotted in Fig. 4 together with

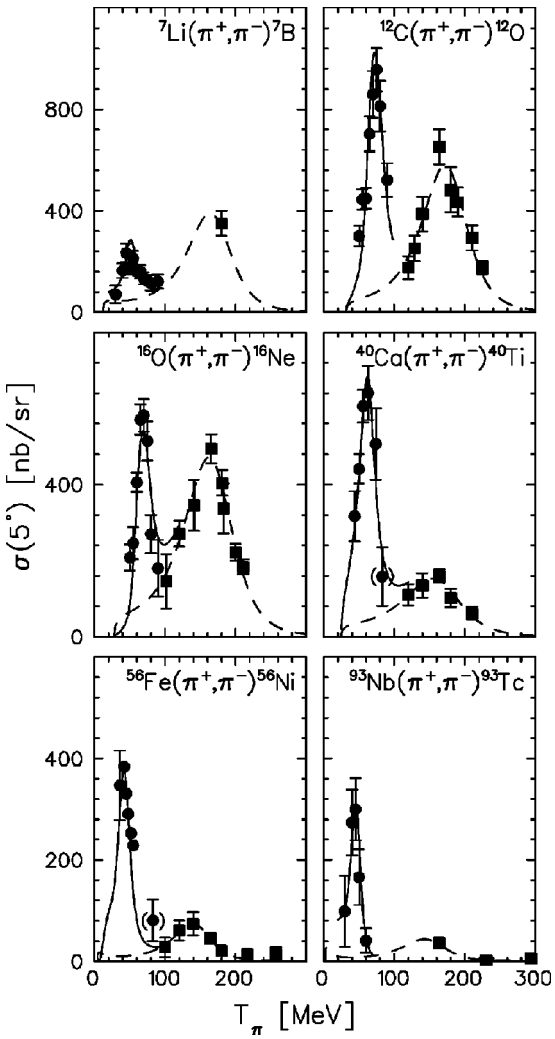

FIG. 1. Energy dependence (lab system) of the forward angle cross section $\sigma(5°)$ of the nonanalog ground state transitions (GST) in ^{7}Li, ^{12}C, ^{16}O, ^{40}Ca, ^{56}Fe, and ^{93}Nb. The data are from this work and from Refs. [10–12,16,26,27,29–31]. Dotted lines represent the $\Delta\Delta$ process in a phenomenological parametrization. The solid curves give the result, when the d' amplitude is added coherently with parameters given in Table II.

the previously published [16,18,25] ones[1] at $T_\pi \approx 50$ MeV. We note, that the previously published data [16,18,25] refer to an incident beam energy of $T_\pi=50$ MeV. However, the midtarget energy is more appropriate. Since for DCX experiments thick targets have to be used in general, the midtarget energies are approximately 1 MeV lower than the incident beam energy. In Table I and in the figures the midtarget energies are given for LEPS measurements. The only exceptions are the already published ^{56}Fe data [16] at $T_\pi=50$ MeV incident beam energy, which are plotted sepa-

[1]A reanalysis of the previous LEPS values [16] revealed an angle dependent normalization error [32] leading to cross sections lower by up to 23%. The corrected values are plotted in Fig. 4 and given in Table I.

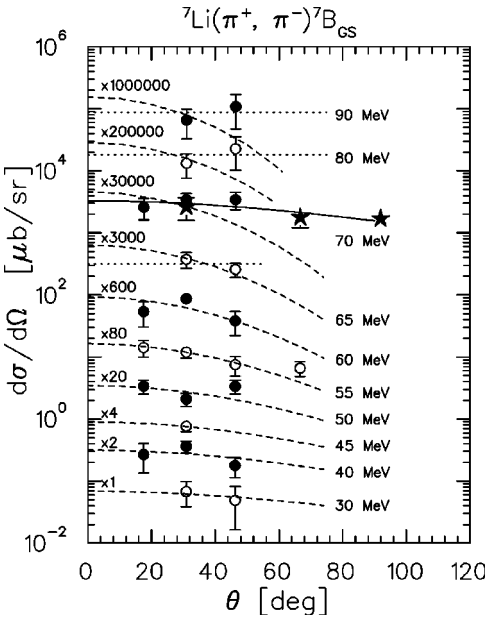

FIG. 2. Angular distributions (lab system) of the GST in ^{7}Li for the energy range $T_\pi = 30$–90 MeV. Open and solid circles refer to data from Ref. [12]; data represented by stars are from this work. The dashed curves represent d' calculations adjusted in height to the data. The dotted horizontal lines characterize an isotropic angular dependence fitted to the data for $T_\pi \geqslant 65$ MeV, and the solid curve is the (nearly isotropic) d' calculation for $T_\pi = 30$ MeV adjusted in height to the data at $T_\pi = 70$ MeV.

rately in Figs. 4(a) and 4(b) together with the LAMPF and TRIUMF results at this incident energy. They should be directly comparable to the new 49 MeV midtarget energy data. For the DIAT they are systematically higher than the new

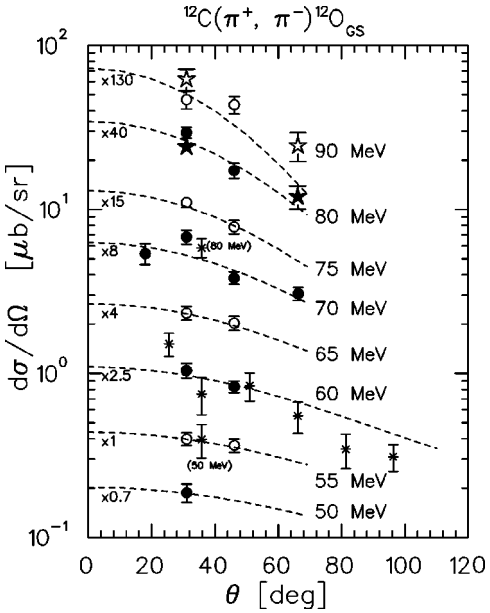

FIG. 3. Same as Fig. 2, but for the GST in ^{12}C. Star and circle symbols denote LEPS measurements at different beam times. Asterisk symbols denote LAMPF data [19] at $T_\pi = 50$, 60, and 80 MeV.

values at this energy, for the GST they are fully compatible with the new data. In addition to DIAT and GST also the nonanalog transition to the (0_2^+, $E_x = 3.96$ MeV) and (0_3^+, $E_x = 5.00$ MeV) states in ^{56}Ni have been observed. They exhibit angular dependences compatible to that of the GST. These data are given in Table I together with all other DCX data measured at LEPS.

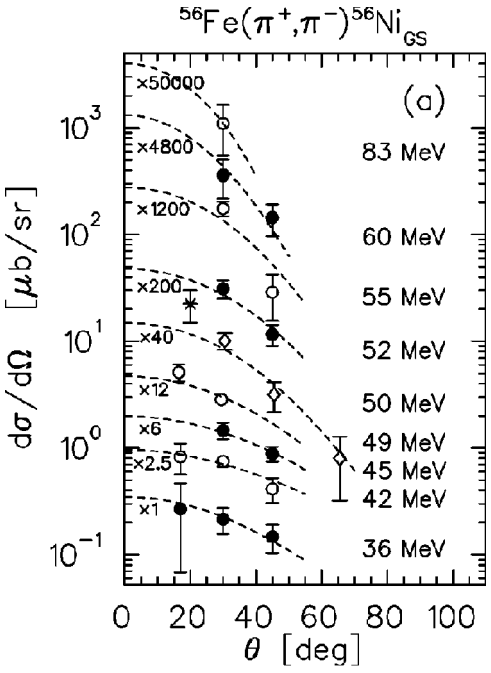

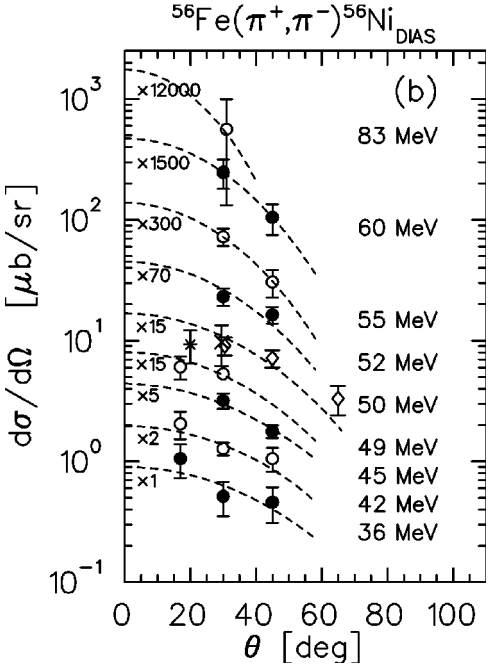

FIG. 4. (a) Same as Fig. 3, but for the GST in ^{56}Fe. Open and solid circles denote LEPS measurements for this work; diamonds are corrected LEPS data (see text) from Ref. [16]; asterisks denote LAMPF [25] data. (b) Same as (a), but for the DIAT in ^{56}Fe. The cross symbol denotes the TRIUMF [18] datum.

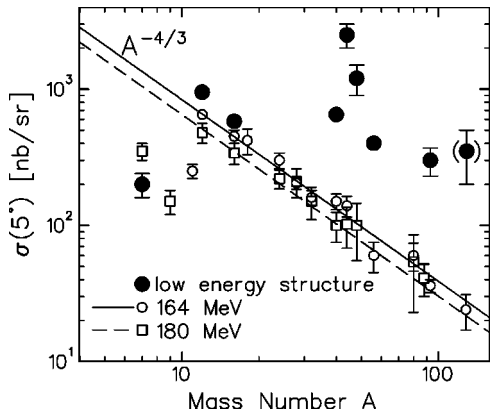

FIG. 5. Systematics of the GSTs in the Δ region and at the peak of the low-energy structure. Open symbols represent the data at $T_\pi = 164$ and 180 MeV [26–31,34], the solid ones the peak forward angle cross sections from Refs. [10–12,14,23] and this work at energies below the Δ-resonance region. Solid and dashed lines give the $A^{-4/3}$ dependence fitted to the data at $T_\pi = 164$ and 180 MeV, respectively, for $A \geqslant 12$.

III. DISCUSSION

A. Energy dependence

Common to all observed monopole transitions is the appearance of a resonancelike structure in the energy dependence of the forward angle cross section. This structure with a width of 20–30 MeV is centered at $T_\pi = 45$–75 MeV depending on the Q value of the transition [10]. The only known exception is the DIAT in ^{48}Ca. Reasons for the nonappearance of this structure there have been presented in Ref. [9]; they essentially rely on the suppression of short-range correlations due to the shell closure in ^{48}Ca and in consequence also in its DIAS [33]. For nonanalog GSTs the structure at low energies is followed by a second, broad bump in the region of the Δ resonance. The latter structure has been successfully explained by the so-called ΔΔ or DINT process [1]. For DIATs there is no second bump at higher energies, since there the sequential single charge exchange proceeding via the IAS in the intermediate nucleus is the dominating process [1]. This process does not resonate in the Δ region, it rather is expected to increase smoothly with increasing energy until it saturates at $T_\pi \approx 300$ MeV in agreement with the observed trend in the DIAT data. Also, since this so-called ''analog route'' is not present in nonanalog transitions, the latter are expected to have much smaller cross sections than the DIATs in general. Hence it is not surprising that the peak-to-valley ratio of the low-energy structure is much more pronounced in the data for GSTs than in those for DIATs. For the discussion of this structure we will therefore concentrate on the GSTs in the following.

Figure 5 shows the forward-angle GST cross sections $\sigma(5°)$ observed at the peak of the low-energy structure versus target mass number. They are compared to the corresponding $\sigma(5°)$ values for the peak in the Δ region, where for $A \geqslant 12$ a simple $A^{-4/3}$ dependence (solid and dashed lines for $T_\pi = 164$ and 180 MeV, respectively) is observed. This dependence is understood as being due to the ΔΔ process in combination with the strong pion absorption in the region of the Δ resonance [1]. The situation for $A < 12$ nuclei is special. The much smaller cross sections observed there have been associated [12,34] with the appearance of a halo structure in the final nuclei, which leads to a much reduced overlap between initial and final state wave functions.

The systematics of the low-energy peak cross sections is quite different from those observed in the Δ region. With the exception of the special case ^{7}Li$(\pi^+\pi^-)^7$B [12] all low-energy data lie well above the Δ-resonance results, in particular for $A \geqslant 40$, and the observed A-dependence is very modest—if there is any at all. However, there are apparent shell structure effects. The GSTs on ^{44,48}Ca have by far the largest cross sections, which is reasonable since these are intrashell transitions, where the overlap between initial and final states is very large. Hence it is also not surprising that their cross sections are nearly as large as those typical for the DIATs (see below and Fig. 3 of Ref. [14]), where the overlap is at optimum. In contrast, the GSTs on ^{56}Fe, ^{93}Nb, and ^{129,130}Te [2] are cross shell transitions having much smaller spatial overlap between initial and final state wave functions. The same holds for the GSTs on ^{16}O and ^{40}Ca, if we ignore that their shell closure is not perfect. This renders it plausible that their cross sections are substantially smaller than those for the intrashell transitions. We note that the $\sigma(5°)$ values observed for the cross shell transitions are all the same within a factor of two. The value for the GST on ^{12}C is slightly higher, which can be related to the fact that ^{12}C is strongly deformed and thus configuration mixed. Hence this GST is partly an intrashell transition, leading to an enhanced cross section for this case.

For the DIATs the systematics of the forward angle cross sections at low energies has been presented already in Refs. [25,14]. The observation there that $\sigma(5°)*(N-Z-1)/(N-Z) \approx$ constant ≈ 2 μb/sr, i.e., approximately independent of A, has been interpreted as the reflection of the dominance of the short-range part of the DCX operator at low energies in contrast to the situation at high energies, where the DIAT systematics points to a dominance of the long-range part [1,3,25].

The nature of the resonancelike excitation function at low energies has long been puzzling. As mentioned in the Introduction, one possible interpretation has been the so-called d' hypothesis assuming the formation of a NN-decoupled πNN resonance with $I(J^P) = \text{even}(0^-)$, $m_{d'} \approx 2.06$ GeV and $\Gamma_{\pi NN} = 0.5$ MeV, in the course of the DCX process. In the nuclear medium this resonance experiences collision damping, which gives rise to a spreading width Γ_s. This together with the Fermi motion of the active nucleons causes a large smearing of the d' resonance increasing its width from 0.5 MeV to 20–30 MeV. Here we present d' calculations, where m, Γ_s as well as a general phase φ_o between resonance and background amplitude have been adjusted to the data. The amplitude for this resonant

[2] We note that the shown extrapolated value is based on a single datum at $\Theta = 30°$ for each isotope, using the theoretical angular dependences of Ref. [7].

process is given [9,10] by the primary resonance amplitude folded with the NN c.m. wave functions for valence nucleons in initial and final nuclear states

$$f_{res}=\left(\frac{2^7}{m_N^3 m_\pi}\right)^{1/2}\frac{a^6}{\pi^2(E_R-m_\pi)^2}\frac{k_R}{k}\left(\frac{k'}{k}\right)^{1/2}\sqrt{\Gamma_+\Gamma_-}\sum_{\substack{NN'nn'L\\ j_1j_2j_1'j_2'}}\left(\int\psi_{n0}(r)e^{-a^2r^2}d^3r\right)\left(\int\psi_{n'0}(r')e^{-a^2r'^2}d^3r'\right)$$

$$\times c_L(j_1j_2)d_{L'}(j_1'j_2')b_{LNn}(j_1j_2)b_{L'N'n'}(j_1'j_2')\int\frac{R_{NL}(q)R_{N'L'}(q')P_L(\cos\beta)P_J(\cos\gamma)}{E-E_R-Q/2-k^2/2m_{d'}-\mathbf{qk}/m_{d'}+i\Gamma/2}d^3q. \quad (1)$$

Here $\Gamma=\Gamma_s+\Gamma_{\pi NN}, \Gamma_+, \Gamma_-\approx\Gamma_+\approx\Gamma_{\pi NN}/3, E_R=m_{d'}-2m_N$ denote total and partial widths as well as the resonance energy of d' in the nuclear medium, and k_R is the pion momentum at resonance. $\Gamma_{\pi NN}$ denotes the vacuum width of d'. R_{NL} and $R_{N'L'}(q$ and $q')$ are the radial wave functions (momenta of the c.m. motion of the NN pair in initial and final nuclear states, whereas $\psi_{n0}(r)$ and $\psi_{n'0}(r')$ describe the relative motion of the two nucleons with $l=0$ and $S=0$ at distance r and r', respectively. N, N', n, n', L, and L' are the quantum numbers for nodes and c.m. angular momentum resulting from the Talmi-Moshinsky transformation [coefficients $b_{LNn}(j_1j_2)$ including $jj\rightarrow LS$ coupling] of the single particle wave functions with j_1 and j_2, and $c_L(d_L)$ denote the two-nucleon coefficients of fractional parentage for initial (final) nuclear states. The angles β and γ appearing in the Legendre polynomials $P_L(\cos\beta)$ and $P_J(\cos\gamma)$ are functions of the momenta q, q', k, and k', where k and k' denote initial and final pion momenta, respectively, and J stands for the spin of d'. Since $S=0, l=0$, we have $L'=L$. For the formation of d' we simply assumed a Gaussian interaction of range $\alpha^{-1}=1$ fm.

The results of these calculations are shown in Figs. 1–4. For ^{7}Li, ^{16}O, ^{40}Ca, and ^{93}Nb they have been discussed already in Refs. [10–12]. For ^{12}C and ^{56}Fe they are new, using simple configuration-mixed wave functions suggested by Refs. [35–37] and [38,39]. To keep things simple the conventional background process at low energies has been assumed throughout these GST calculations to arise solely from the tail of the $\Delta\Delta$ process. For the latter we adopt a phenomenological description [40] with a phase running from 0° to 360° due to the double resonance nature of this process [1]. In Fig. 1 the contribution of the $\Delta\Delta$ process is depicted by the dashed curves. The solid lines are obtained by the coherent addition of the d' amplitude with parameters given in Table II. The adjusted values for the spreading width Γ_s vary between 10–20 MeV, with the smaller value occuring preferentially for light nuclei. The effective mass of d' in the nuclear medium $m_{d'}$ is seen to vary only within a few MeV, its value, however, is somewhat correlated to the choice of the phase φ_o between both processes. This is illustrated by two sets of parameters for the GST on ^{16}O in Table II, which give comparable descriptions of the data. Also shown in the table is a fit parameter f, which scales the d' amplitude for an optimal description of the data. It is different from unity only for the GSTs on ^{12}C, ^{56}Fe, and ^{93}Nb, i.e., for cases where configuration mixing is important. Since we have used only the dominant configurations for the d' calculations for simplicity, it is not surprising that these cross sections are too low, since configuration mixing may enhance the d' amplitude considerably [10]. Of course, there could also be other reasons for $f\neq1$ such as, e.g., a shortcoming of the description of the conventional process at low energies. It should be stressed also, that the d' calculations do not include pion distortions in entrance and exit channels. Estimates of their effect range from 10% [33] to a factor of 2 [3,5] enhancement in the DCX cross section at low energy. Hence, distortions could significantly enhance the d' amplitude and thus effectively reduce the value of $\Gamma_{\pi NN}=0.5$ MeV required so far for the description of the data. We note also that our assumption of the conventional GST background to be just the tail of the $\Delta\Delta$ process implies that the conventional sequential process yields negligible contributions to the cross shell transitions under consideration. If this is not valid, then the d' amplitude (and with it $\Gamma_{\pi NN}$) would have to be reduced further in order to comply with the data.

B. Angular dependence

The measured angular distributions shown in Figs. 2–4 for the GSTs in ^{7}Li, ^{12}C, ^{56}Fe and the DIAT in ^{56}Fe exhibit a smooth fall-off with the pion scattering angle. Also, the fall-off is increasing with increasing incident energies, until the dip region between the low-energy and the $\Delta\Delta$ bump is reached. This diffractive behavior is observed in all measured DCX transitions and simply reflects the nuclear size, more exactly the center-of-mass motion of the active nucleon

TABLE II. Parameters of the d' amplitude used for the description of the forward angle cross sections in Figs. 1 and 6.

Transition	$m_{d'}$	Γ_s	φ_o	f
^{7}Li GST	2060	10–15	−60°	1
^{12}C GST	2070	10	−30°	1.3
^{16}O GST	2065	10	−90°	1
	(2070	10	0°	1)
^{40}Ca GST	2065	20	0°	1
^{56}Fe GST	2060	20	−60°	2
^{93}Nb GST	2060	15	110°	2.1
^{42,44,48}Ca GST,DIAT	2065	20	−90°	1

pair [33]. Hence both d' calculations as well as conventional calculations, which account for this motion of the nucleon pair, predict very similar angular dependences [9]. The dashed curves in Figs. 2–4 show d' calculations adjusted in absolute height for best reproduction of the data. They account very well for the observed angular dependences at least up to the dip region. There the situation may change as the data for ^{7}Li, ^{12}C, and ^{16}O suggest. Unfortunately these are the only transitions where cross sections in the dip region have been measured at more than one angle. If the observation of a very flat angular dependence in the dip region for the above three cases is valid generally, then also the extrapolated $\sigma(5°)$ value of the GST in ^{56}Fe at $T_\pi = 83$ MeV (Fig. 1) has to be questioned very much. As seen in Fig. 4, we assumed an already quite steeply rising d' angular dependence. Assuming a flat dependence instead would bring the $\sigma(5°)$ value down by up to a factor of 3 resulting in much better agreement with the neighboring $T_\pi = 100$ MeV value measured with the EPICS spectrometer at LAMPF [30]. Hence we have put the $T_\pi = 83$ MeV values in brackets in Fig. 1 both for ^{40}Ca and ^{56}Fe.

C. Ca isotopes revisited

As already pointed out in the Introduction, there are very recent theoretical calculations [13], which for the first time provide a nearly quantitative description of the data on the intrashell transitions in the ^{42,44,48}Ca isotopes both in their energy and angular dependence. By fine tuning the optical model parameters and using the closure approximation for the excitation of the intermediate states in the sequential process Nuseirat *et al.* [13] gain about a factor of 2 in the calculated cross sections compared to previous calculations [3], which brings these conventional calculations close to the data. They emphasize, however, that the calculated energy dependences do not resemble a resonancelike behavior. In case of ^{42}Ca it is more a flat-topped bump (dotted curve in Fig. 6). Unfortunately the statistical accuracy of the LAMPF data taken only at a few energies for these Ca isotopes does not allow to discriminate between the different predicted shapes in the energy dependence. Also for these intrashell transitions the predicted d' effect is rather small. The solid line in Fig. 6 shows the effect, if we add the d' amplitude coherently to that of Nuseirat *et al.* Though the effect is small, it is able to improve the description of the data still somewhat. The situation is similar for the other intrashell transitions in the Ca isotopes [41]. We note that in the early d' calculations [9] for these transitions the predicted d' effect was much bigger, since there $\Gamma_s = 5$ MeV was assumed. However, the subsequent PSI measurements on GSTs (Fig. 1) clearly showed that this value is much too small—in agreement with theoretical estimates [10] that appeared by then. The subsequent readjustment of Γ_s by a factor of 4 as well as the Q-value correction [see Eq. (1)] introduced in Ref. [10] decreased the d' effect now to that shown in Fig. 6.

Its contribution to the peak cross section in ^{42}Ca amounts to $\lesssim 1$ μb/sr. This roughly equals the measured peak cross section for the closed shell nuclei ^{16}O and ^{40}Ca, which are well described by the d' process alone (see Fig. 1). Therefore it will be interesting to see if these cases can be successfully described in terms of the conventional mechanism.

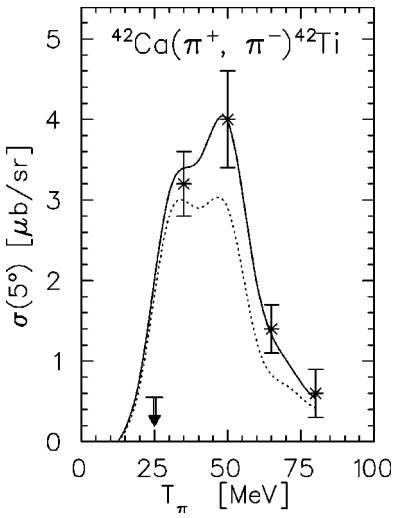

FIG. 6. Energy dependences of the forward angle cross section for the DIAT in ^{42}Ca. The data are from LAMPF [23]. The dotted line represents the calculations of Ref. [13] for the conventional sequential process. The solid line gives the result, when the d' amplitude is added coherently with parameters given in Table II.

D. Very light nuclei

^{7}Li is the lightest nucleus where the DCX reaction can proceed to a discrete final state. For still lighter target nuclei the DCX reaction can proceed only to the nuclear continuum. With regard to d' this means that it no longer can be formed off-shell in the presence of $A-2$ nucleons, it only can be produced on-shell associatedly with the simultaneous release of spectator nucleons into the continuum. Hence the d' signature for the DCX into the continuum is expected to be much less pronounced. Nevertheless new detailed DCX continuum measurements have been carried out on ^{3}He [42] and ^{4}He [42,43] with the aim to search among other things for possible d' signatures there. Unfortunately also here the original d' predictions turned out much too optimistic. The revised large value for the spreading width leads to a strong reduction of the expected d' signal such that the new data on ^{3}He and ^{4}He cannot establish unambiguously the presence or absence of a d' signal.

IV. SUMMARY

With these new measurements there exists now a solid basis of data for the low-energy DCX to discrete final states in nuclei, ranging from the lightest nucleus, where such a reaction is possible, up to ^{93}Nb and Te. All investigated transitions with the well-known exception of the DIAT in ^{48}Ca exhibit a 20–30 MeV broad structure near $T_\pi = 45 - 70$ MeV—depending on the reaction Q value—in the energy excitation function of the forward angle cross section. This structure is particularly pronounced in the GSTs. Their peak cross sections show clear shell structure effects with intra shell transitions being much larger than cross shell tran-

sitions. In contrast to the situation in the Δ-resonance region the *A* dependence observed at low energies is very weak, if there is any at all. This observation is in accordance with that for the DIATs discussed in Refs. [25,14].

The measured angular distributions behave regularly, i.e., as expected for a diffractive process, at least up to the dip region between the low-energy structure and the Δ bump.

The data across the low-energy structure can be reasonably well described by the d' hypothesis, i.e., the formation of a narrow πNN resonance in the course of the DCX process. Alternatively recent conventional calculations of Nuseirat *et al.* [13] for the first time are able to account for the energy and angle dependence observed for the intra shell transitions in the Ca isotopes. The authors emphasize, however, that their calculations predict structures in the energy dependence which are much different from that expected for a resonance. On the other hand our GST measurements, in particular the rather detailed ones on ^{12}C, ^{16}O, and ^{40}Ca, clearly reveal such a resonancelike shape. Hence it will be very interesting to see whether the systematic data presented here will allow discrimination between such conventional calculations and the d' ansatz.

ACKNOWLEDGMENTS

This work has been supported by the German Federal Minister for Education and Research (BMBF) under Contracts No. 06 TU 886, 06 TU 987 and by the DFG Graduiertenkolleg (Mu 705/3).

[1] For a survey see, e.g., M. B. Johnson and C. L. Morris, Annu. Rev. Nucl. Part. Sci. **43**, 165 (1993); H. Clement, Prog. Part. Nucl. Phys. **29**, 175 (1992), and references therein.
[2] G. A. Miller, Phys. Rev. Lett. **53**, 2008 (1984); Phys. Rev. C **35**, 377 (1987).
[3] N. Auerbach, W. R. Gibbs, N. J. Ginocchio, and W. B. Kaufmann, Phys. Rev. C **38**, 1277 (1988).
[4] E. R. Siciliano, M. B. Johnson, and H. Sarafian, Ann. Phys. (N.Y.) **203**, 1 (1990).
[5] M. A. Kagarlis and M. B. Johnson, Phys. Rev. Lett. **73**, 38 (1994).
[6] M. B. Johnson *et al.*, Phys. Rev. C **44**, 2480 (1991).
[7] Y. Liu, A. Faessler, J. Schwieger, and A. Bobyk, J. Phys. G **24**, 1135 (1998).
[8] R. Bilger *et al.*, Z. Phys. A **343**, 491 (1992).
[9] R. Bilger, H. A. Clement, and M. G. Schepkin, Phys. Rev. Lett. **71**, 42 (1993); **72**, 2972 (1994).
[10] K. Föhl *et al.*, Phys. Rev. Lett. **79**, 3849 (1997).
[11] J. Pätzold *et al.*, Phys. Lett. B **428**, 18 (1998).
[12] J. Pätzold *et al.*, Phys. Lett. B **443**, 77 (1998).
[13] M. Nuseirat *et al.*, Phys. Rev. C **58**, 2292 (1998); W. R. Gibbs (private communication).
[14] K. Föhl *et al.*, Phys. Rev. C **53**, R2033 (1996).
[15] B. M. Barnett *et al.*, Nucl. Instrum. Methods Phys. Res. A **297**, 444 (1990); H. Matthäy *et al.*, in *Proceedings of the International Symposium on Dynamics of Collective Phenomena in Nuclear and Subnuclear Long Range Interactions in Nuclei*, Bad Honnef, 1987, edited by P. David (World Scientific, Singapore, 1988), p. 542.
[16] R. Bilger *et al.*, Phys. Lett. B **269**, 247 (1991).
[17] I. Navon *et al.*, Phys. Rev. Lett. **52**, 105 (1984).
[18] A. Altman *et al.*, Phys. Rev. Lett. **55**, 1273 (1985); T. Anderl, doctoral thesis, University of Bonn, 1988.
[19] J. A. Faucett *et al.*, Phys. Rev. C **35**, 1570 (1987).
[20] M. J. Leitch *et al.*, Phys. Rev. C **39**, 2356 (1989), and references therein
[21] H. W. Baer *et al.*, Phys. Rev. C **35**, 1425 (1987); **43**, 1458 (1991).
[22] Z. Weinfeld *et al.*, Phys. Rev. C **37**, 902 (1988); Phys. Lett. B **237**, 33 (1990).
[23] M. J. Leitch *et al.*, Phys. Lett. B **294**, 157 (1992).
[24] J. D. Silk *et al.*, Phys. Rev. C **51**, 665 (1995).
[25] H. Ward *et al.*, Phys. Rev. C **47**, 687 (1993).
[26] K. K. Seth, in *Second LAMPF International Workshop on Pion-Nucleus Double Charge Exchange*, Los Alamos, 1989, edited by W. R. Gibbs and M. J. Leitch (World Scientific, Singapore, 1990), p. 473.
[27] L. C. Bland *et al.*, Phys. Lett. **128B**, 157 (1983).
[28] R. Gilman *et al.*, Phys. Rev. C **34**, 1895 (1986), and references therein.
[29] D. L. Watson *et al.*, Phys. Rev. C **43**, 1318 (1991).
[30] P. A. Seidl *et al.*, Phys. Rev. C **42**, 1929 (1990), and references therein.
[31] M. A. Kagarlis *et al.*, Phys. Rev. C **47**, 1219 (1993).
[32] K. Föhl, doctoral thesis, University of Tübingen, 1996.
[33] E. Bleszynski, M. Bleszynski, and R. J. Glauber, Phys. Rev. Lett. **60**, 1483 (1988); Phys. Rev. C **36**, 681 (1987).
[34] W. R. Gibbs and A. C. Hayes, Phys. Rev. Lett. **67**, 1395 (1991); T. Kabayashi, Nucl. Phys. **A538**, 343c (1992); **A553**, 465c (1993).
[35] W. B. Cottingame *et al.*, Phys. Rev. C **36**, 230 (1987).
[36] W. Bauhoff *et al.*, Nucl. Phys. **A410**, 180 (1983).
[37] K. Amos and I. Morrison, Phys. Rev. C **19**, 2108 (1979).
[38] H. Horie and K. Ogawa, Nucl. Phys. **A216**, 407 (1975).
[39] P. Halse, Phys. Rev. C **41**, 2340 (1990).
[40] R. Gilman *et al.*, Phys. Rev. C **35**, 1334 (1987).
[41] J. Draeger, graduation thesis, University of Tübingen, 1999.
[42] J. Gräter *et al.*, Phys. Lett. B **471**, 113 (1999).
[43] J. Gräter *et al.*, Phys. Lett. B **420**, 37 (1998); Phys. Rev. C **58**, 1576 (1998).